Journal of Magnetism and Magnetic Materials 321 (2009) 3159–3163

Contents lists available at ScienceDirect

Journal of Magnetism and Magnetic Materials

journal homepage: www.elsevier.com/locate/jmmm

Thermomagnetic transitions and coercivity mechanism in bulk composite $Nd_{60}Fe_{30}Al_{10}$ alloys

R. Ortega-Zempoalteca, I. Betancourt *, R. Valenzuela

Departamento de Materiales Metálicos y Cerámicos, Instituto de Investigaciones en Materiales, Universidad Nacional Autónoma de México, México D.F. 04510, Mexico

ARTICLE INFO

Article history:
Received 12 April 2009
Received in revised form
14 May 2009
Available online 22 May 2009

PACS:
75.20.−g
75.30.−m
75.50.Kj
75.60.−d

Keywords:
Hard magnetic alloy
Composite material
Amorphous phase

ABSTRACT

The thermomagnetic behaviour (within the temperature range 553–300 K) for the bulk composite $Nd_{60}Fe_{30}Al_{10}$ alloy is described in terms of a transition from paramagnetic to superferromagnetic state at $T = 553$ K, followed by a ferromagnetic ordering for $T < 473$ K. For the superferromagnetic regime, the alloy thermomagnetic response was associated to a homogeneous distribution of magnetic clusters with mean magnetic moment and size of $1072\,\mu_B$ and 2.5 nm, respectively. For $T < 473$ K, a pinning model of domain walls described properly the alloy coercivity dependence with temperature, from which the domain wall width and the magnetic anisotropy constant were estimated as being of ≈ 8 nm and $\approx 10^5$ J/m^3, typical values of hard magnetic phases. Results are supported by microstructural and magnetic domain observations.

1. Introduction

Hard magnetic materials based on RE–TM–Al (RE = Nd, Pr, Sm, Gd; TM = Fe, Co) alloys have elicited a considerable interest from both, the scientific and technical point of view because of their high coercivity values arising from the interplay between amorphous/secondary crystalline phases, and the possibility of preparing bulk materials in excess of 10 mm of diameter in rod-shaped samples by means of a simple copper-mold casting techniques [1–5]. The microstructure, as well as the magnetic properties in the as-quenched metallic samples are largely determined by the cooling rate used to solidify these alloys from the melt, since the magnetic behaviour may change from coercive materials (typically ~300 kA/m) prepared at low cooling rates ($< 10^2$ K/s, typical of die-casting process), to soft magnetic-like alloys (with coercivities below 10 kA/m) obtained at much higher cooling rates (typically between 10^5 and 10^6 K/s, characteristic of rapid solidification techniques, such as melt spinning) [2,4,5].

Although, there is no unanimous agreement on the coercivity mechanism of these RE–TM–Al-based alloys because of the variety of microstructures and phase distribution described profusely in the specialized literature (from single amorphous phase [1–5] to nanocomposite material having a nanophase crystallite distribution embedded in a majority amorphous matrix [6–10]), a common characteristic for all the microstructures observed is the presence of an homogeneous distribution of nanosized exchange coupled Fe-rich clusters [3–5,11–14], whose average size (between 2 and 5 nm) would be a measure of a correlation length l. On the other hand, the inter-cluster exchange interaction implies an exchange length $l_{ex} = (A/K)^{1/2}$ (A = exchange constant, K = anisotropy constant), such that when $l \approx l_{ex}$, the local magnetic vector is strongly constrained by the orientation of the local anisotropy and hard magnetic properties arise. A complementary view considering a composite structure leads to the formation of magnetic domains due to the inter-cluster exchange interaction, and hence, the coercivity becomes the result of a pinning process at the secondary crystalline phases.

In this work, we describe the coercivity of $Nd_{60}Fe_{30}Al_{10}$ bulk alloys with composite microstructure in terms of the thermomagnetic behaviour of the clustered amorphous phase, magnetic domain formation and their interaction with pinning sites.

2. Experimental methods

The master alloy ingot with composition $Nd_{60}Fe_{30}Al_{10}$ was prepared by arc-melting the pure component elements within inert argon atmosphere. Bulk cylindrical rods (3 mm diameter × 50 mm length) were obtained from the master alloy by die-casting process into a copper mold under argon atmosphere. The microstructure of

* Corresponding author. Tel.: +52 55 56224654; fax: +52 55 56161371.
E-mail address: israelb@correo.unam.mx (I. Betancourt).

0304-8853/$ - see front matter © 2009 Elsevier B.V. All rights reserved.
doi:10.1016/j.jmmm.2009.05.032

as-cast cylinders was characterized by transmission electron microscopy. The alloy magnetic structure was determined by means of magnetic force microscopy (MFM). On the other hand, magnetic measurements were carried out using a Vibrating Sample Magnetometer (VSM) within the temperature range 300–553 K with a maximum applied field H_{max} of 1360 kA/m.

3. Results

The composite character of the bulk $Nd_{60}Fe_{30}Al_{10}$ is manifested in Fig. 1, for which the TEM image shows some fine crystallites of hcp Nd, as indicated by the corresponding selected area diffraction pattern SADP, for which the (101), (104), (105) and (107) planes were identified. The mean size of the Nd crystallites is ~20 nm and they appear embedded in an amorphous phase, as is evidenced by the diffuse haloes and circularly arranged dots present in the SADP. On the other hand, the room-temperature magnetisation M–H curve for a bulk composite $Nd_{60}Fe_{30}Al_{10}$ alloy sample is shown in Fig. 2 exhibiting the following properties: maximum magnetisation $\mu_0 M_{max}$ of 0.19 T, remanence magnetisation $\mu_0 M_r$ of 0.13 T and intrinsic coercivity H_c of 282 kA/m. Further magnetisation curves with increasing temperature T were recorded within the range 300–553 K, from which $\mu_0 M_r$ and H_c as a function of T are displayed in Fig. 3 exhibiting an expected decreasing tendency for both properties as the temperature rises and becomes zero at $T_1 = 473$ K. Beyond this temperature, the M–H plots manifest anhysteretic character, as it is shown in Fig. 4, for which a fully paramagnetic state is manifested up to $T_2 = 553$ K.

4. Discussion

As mentioned in the precedent introduction section, the amorphous phase is a characteristic of bulk RE–TM–Al alloys,

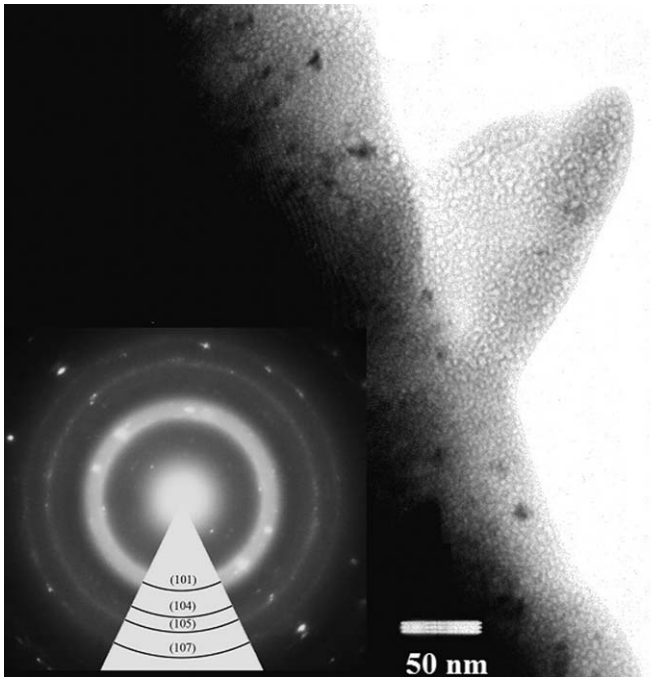

Fig. 1. Electron microscopy micrograph corresponding to a bulk $Nd_{60}Fe_{30}Al_{10}$ alloy sample showing the presence of small hcp Nd precipitates (for which the (101), (104), (105) and (107) planes were indexed in the corresponding SADP) having a mean grain size of about 20 nm.

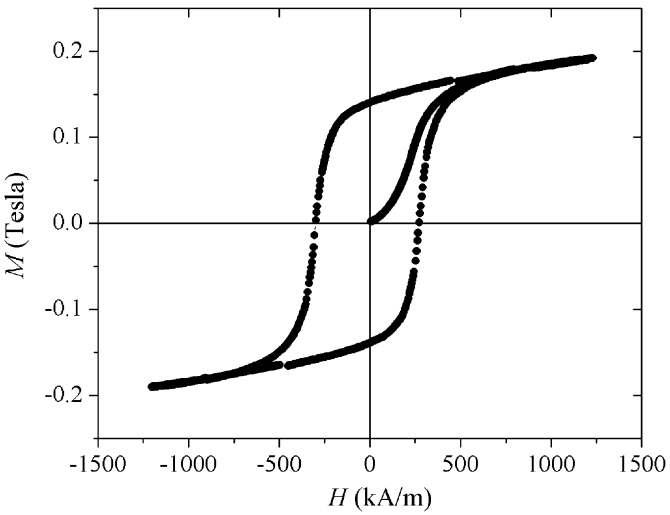

Fig. 2. M–H curves for the $Nd_{60}Fe_{30}Al_{10}$ bulk alloy at room temperature.

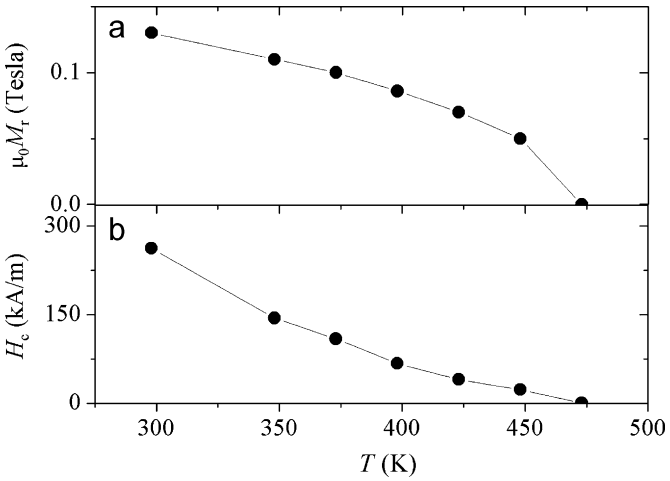

Fig. 3. Remanence magnetisation (a) and coercivity field (b) as a function of temperature for the $Nd_{60}Fe_{30}Al_{10}$ bulk alloy (solid lines represent a guide for the eye, only).

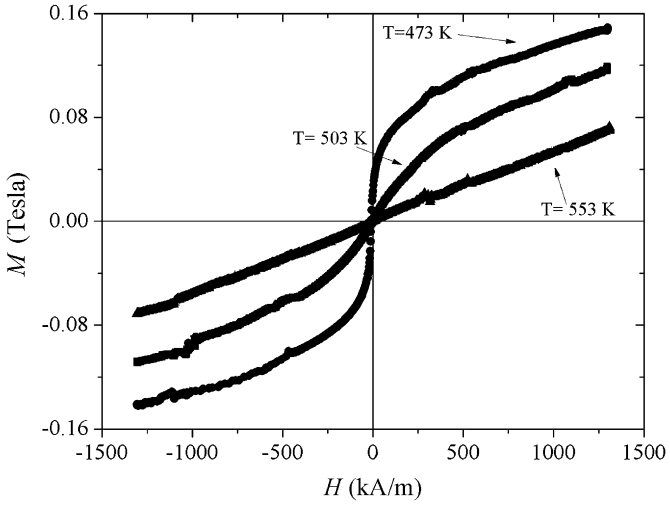

Fig. 4. M–H curves for the $Nd_{60}Fe_{30}Al_{10}$ bulk alloy at 473, 503 and 553 K.

and it has been described as encompassing an homogeneous distribution of nanosized (1–3 nm) exchange-coupled Fe-rich clusters as a result of the relaxed amorphous structure afforded by the low cooling rate of the simple casting process used [11–16]. Due to the minute dimension of these clusters, they must possess a single domain character, and hence are also susceptible to present a superparamagnetic behaviour before the transition to a fully paramagnetic state. According to our findings, this is the case for the current bulk $Nd_{60}Fe_{30}Al_{10}$ alloy as pointed out by the absence of hysteresis between 473 and 553 K (Fig. 4). This anhysteretic behaviour is analyzed in the following.

For a collection of superparamagnetic entities with magnetic moment m and nil inter-particle interaction, the magnetisation M can be described by [17]:

$$M = NmL\left(\frac{mH}{k_BT}\right) \tag{1}$$

where N is the number of clusters per unit volume; m = spontaneous magnetic moment of each cluster; $L(x)$ = Langevin function; H = applied field; k_B = Boltzmann constant and T = temperature of measurement. By assuming ferromagnetic coupling between atom spins within each cluster, it is reasonable to expect a temperature dependence of m, i.e. $m = m(T)$ [18,19], where

$$m(T) = m_s b\left(\frac{T}{T_c^{\text{clust}}}\right) \tag{2}$$

with m_s = saturation magnetic moment at 0 K; T_c^{clust} = Curie temperature of the whole clustered phase and $b(T/T_c^{\text{clust}})$ as the temperature dependence function describing the decreasing tendency of magnetisation with increasing temperature, which can be determined on the basis of the Brillouin function for Fe atoms with magnetic moment $\mu_{Fe} \approx 2\,\mu_B$ (established by Mössbauer experiments for analogous melt-spun $Nd_{60}Fe_{30}Al_{10}$ alloys in Ref [8]. μ_B = Bohr magneton). Therefore,

$$M = Nm_s b\left(\frac{T}{T_c^{\text{clust}}}\right) L\left(\frac{m_s b(T/T_c^{\text{clust}})H}{k_BT}\right) \tag{3}$$

For validation of this superparamagnetic model through Eq. (3), $M/b(T/T_c^{\text{clust}})$ vs $b(T/T_c^{\text{clust}})H/T$ curves should converge into a single plot for any combination of H or T with T_c^{clust} as a free parameter [18,19]. For instance, Fig. 5 displays the fitting process of Eq. (3) by using initial M–H plots at variable temperature and $T_c^{\text{clust}} = 553$ K, for which a lack of coincidence between thermomagnetic data and Eq. (3) is manifested.

A variation of the superparamagnetic model described above, proposed for thermomagnetic studies in melt-spun $Pr_{100-x}Fe_x$ and $Y_{60}Fe_{30}Al_{10}$ alloys [18,19], considers the incorporation of an inter-particle interaction in the form of a molecular field wM acting between ferromagnetic clusters, thus resulting in a *superferromagnetic* interaction. Within this frame, the magnetisation $M(T,H)$ becomes

$$M(T,H) = Nm_s b\left(\frac{T}{T_c^{\text{clust}}}\right) L\left(\frac{m_s b(T/T_c^{\text{clust}})(H+wM)}{k_BT}\right) \tag{4}$$

For this equation to be applicable to the present case, $M/b(T/T_c^{\text{clust}})$ vs $b(T/T_c^{\text{clust}})(H+wM)/T$ curves should coincide into a single curve this time with w and T_c^{clust} as free parameters for fitting process [18,19]. For same alloy thermomagnetic data at $H_{max} = 1360$ kA/m, the combination $T_c^{\text{clust}} = 553$ K and $w = 7.5$ leads to a very good agreement with Eq. (4), as shown in Fig. 6. These fitted parameters are in rough agreement with the ones determined for the related melt-spun $Nd_{60}Fe_{30}Al_{10}$ ribbons at 5 m/s: $T_c^{\text{clust}} = 570$ K and $w = 8$, respectively [20].

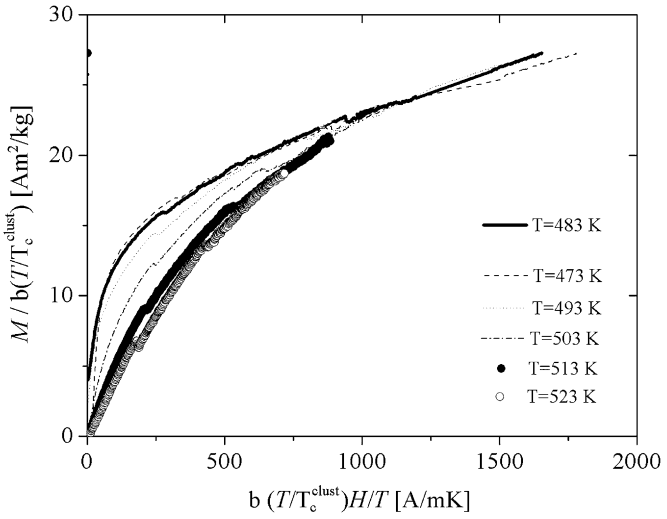

Fig. 5. Fitting of Eq. (3) for initial M–H plots and variable temperature for the $Nd_{60}Fe_{30}Al_{10}$ bulk alloy.

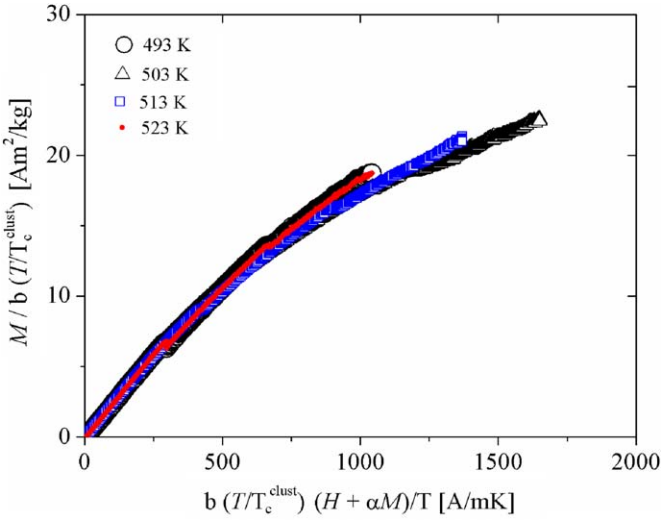

Fig. 6. Fitting of Eq. (4) for initial M–H plots and variable temperature for the $Nd_{60}Fe_{30}Al_{10}$ bulk alloy.

Additionally, when $x \ll 1$, the Langevin function $L(x)$ can be approximated using a series expansion as $L(x) \approx x/3$, so that Eq. (4) becomes

$$M(T,H) = Nm_s^2 b^2\left(\frac{T}{T_c^{clust}}\right)\frac{[H+wM]}{3k_BT} \tag{5}$$

Considering the saturation magnetisation M_0 (at 0 K) as $M_0 = Nm_s$, we have for m_s

$$m_s = \frac{3k_B}{M_0}\left[\frac{M(T,H)T}{b^2(T/T_c^{\text{clust}})(H+wM)}\right] \tag{6}$$

where the term into brackets corresponds to the initial slope of the Langevin data fitting of Fig. 6. For the present case and considering an alloy density of 7.7 g/cm^3, such slope was determined as 184.8 K. Furthermore, experimental measurements at very low temperatures and very high applied magnetic field [21] afford an estimation of $\mu_0 M_0$ as 0.77 T. Therefore, according to Eq. (6), we have for m_s

$$m_s = 9.936 \times 10^{-21}\text{J/T} = 1072\mu_B \tag{7}$$

where $\mu_B = 0.927 \times 10^{-23}$ J/T. For this value of m_s, and reminding that $\mu_{Fe} \approx 2\,\mu_B$ [8], the number of Fe atoms in a cluster can be estimated as $m_s\ [\mu_B]/(2\,\mu_B/\text{atom}) = 536$ atoms. Additionally, an assessment of the number of clusters per unit volume N follows from:

$$N = \frac{M_0}{n\mu_B} \tag{8}$$

where $n =$ number of Bohr magnetons. Present data for M_0 (6.13×10^5 A/m), n (1072) and μ_B leads to $N = 6.16 \times 10^{25}$ clusters/m^3. For this value of N, we would have in a box of $10 \times 10 \times 10\,\text{nm}^3$ about 62 clusters, which imply $\sqrt[3]{62} \approx 4$ clusters per box side, and thus, each one with an average size of ≈ 2.5 nm. This estimation of cluster size is in excellent agreement with high-resolution TEM observations in similar bulk $Nd_{65}Fe_{25-x}Co_xAl_{10}$ and melt-spun $Nd_{60-2/3x}Fe_{30-1/3x}Al_{1+x}$ alloys [22,23] and also with the related high coercive $Pr_{100-x}Fe_x$ amorphous ribbons with a clustered structure verified by HRTEM [18].

For temperatures below $T_1 = 473$ K, the alloy becomes ferromagnetic. Within this magnetically ordered state, the exchange interaction strengthening affords the formation of ferromagnetic domains, as shown in Fig. 7a, which corresponds to a room-temperature MFM image exhibiting clear contrast between adjacent regions, presumably, the magnetic domains. According to image brightness analysis on a $522 \times 522\,\text{nm}^2$ section (Fig. 7b), the transition between dark-clear regions occurs in a progressive way, as indicated by the colour scale: blue for one magnetic orientation and green for the opposite direction, with a black transition zone estimated as being of 10 ± 1 nm in average length (after analyzing several MFM images). This transition length should be associated to the domain wall (DW) width δ_w. Very similar magnetic domain structures were reported for comparable bulk $Nd_{65}Fe_{25-x}Co_xAl_{10}/Nd_{60}Fe_{20}Co_{10}Al_{10}$ alloys [22,24].

Concerning the coercivity mechanism active for this $Nd_{60}Fe_{30}Al_{10}$ bulk alloys, the pinning of domain walls would be consistent with the low initial susceptibility observed in Fig. 2. To test the validity of this assumption, a coercivity model proposed by Gaunt [25] is used to describe the H_c dependence with temperature: According to this model, a material whose coercivity mechanism is driven by the pinning of domain walls at a random array of magnetic inhomogeneities (such as non-magnetic precipitates, inclusions, cavities or any region with different magnetic properties with respect to the main matrix) has an $H_c(T)$ variation that must fit the non-linear relationship

$$H_c^{1/2}(T) = H_0^{1/2} - \left[\frac{75k_B}{4bf}\right]^{2/3} T^{2/3} \tag{9}$$

where H_0 is the applied field necessary to release a DW from a pinning centre in the absence of thermal activation; k_B is the Boltzmann constant; T is the absolute temperature; $4b =$ range of pin interaction $=$ domain wall width δ_w;and $f =$ maximum restoring force per pin. From Eq. (9), it is clear that when thermal activation is neglected ($T = 0$) the material coercivity is given by H_0. However, at any $T > 0$ K, the thermal energy available acts as an activation energy supply, which in turn affords the DW to break away from its pinned position at a field $H < H_0$. The condition for strong pinning (i.e. a single obstacle interacting with a DW for each pining–unpinning process) is satisfied when [25]

$$\frac{3f}{2\pi\gamma\delta_w} > 1 \tag{10}$$

with $\gamma =$ domain wall energy per unit area. This condition is fulfilled for large f/γ ratio or for small δ_w, which requires narrow DW (small δ_w), and thus, a large magnetic anisotropy constant K.

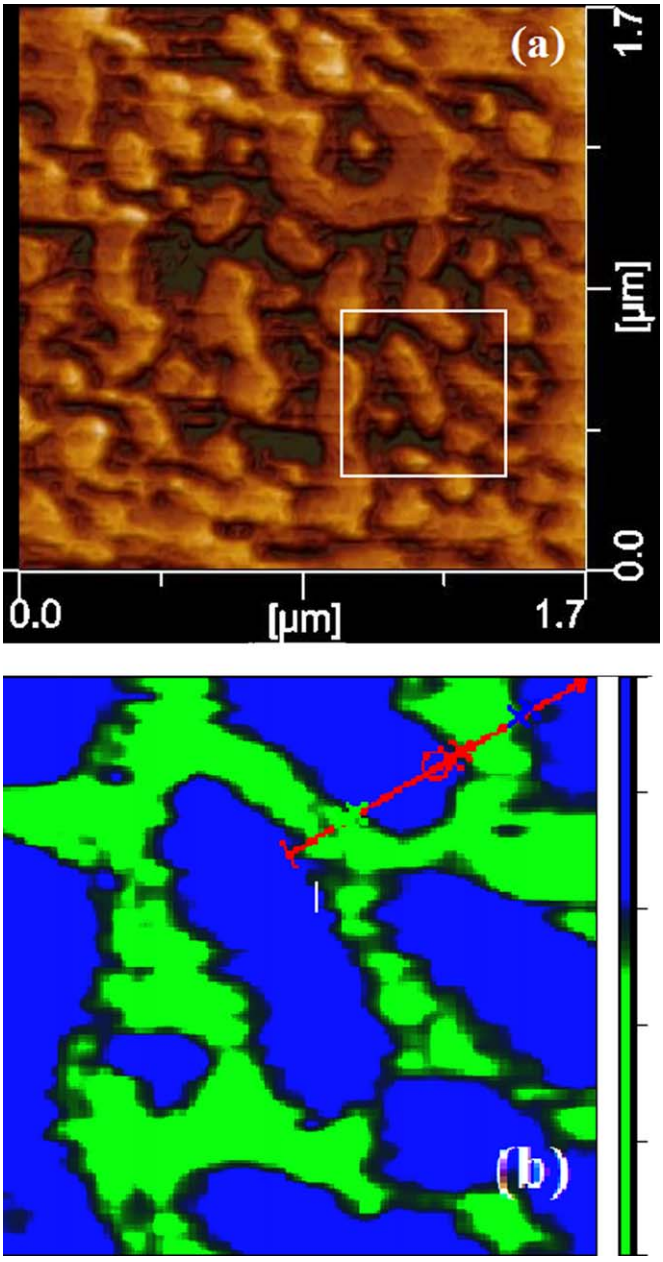

Fig. 7. MFM image at room temperature for the $Nd_{60}Fe_{30}Al_{10}$ bulk alloys showing (a) magnetic domain formation within an area of $1.7 \times 1.7\,\mu\text{m}^2$ and (b) a detailed structure from the white square in (a) showing the progressive transition from one domain direction (green scale, on the right) to the opposite one (blue scale), with a transition zone (in black) 10 ± 1 nm. The thickness of the transition between adjacent domains is indicated along the red line. (For interpretation of the references to colour in this figure legend, the reader is referred to the web version of this article.)

For the present case, the pinning centres were associated to the secondary paramagnetic Nd-rich crystallites observed by TEM (Fig. 1). Fitting of $H_c(T)$ data (Fig. 3) with Eq. (9) between 300 and 463 K (i.e. well before the onset of the superferromagnetic regime) is shown in Fig. 8, exhibiting an excellent agreement, which resulted in the following expression after minimum square processing: $H_c^{1/2} = 1.8656\ [T^{1/2}] - 0.0289T^{2/3}\ [T^{1/2}K^{-2/3}]$.

According to Eq. (9), the critical field H_0 can be determined as $H_0 = (1.8656\,T^{1/2})^2 = 3.48$ T, which is in excellent agreement with experimental measurements at low temperatures ($H_0 = 3.5$ T

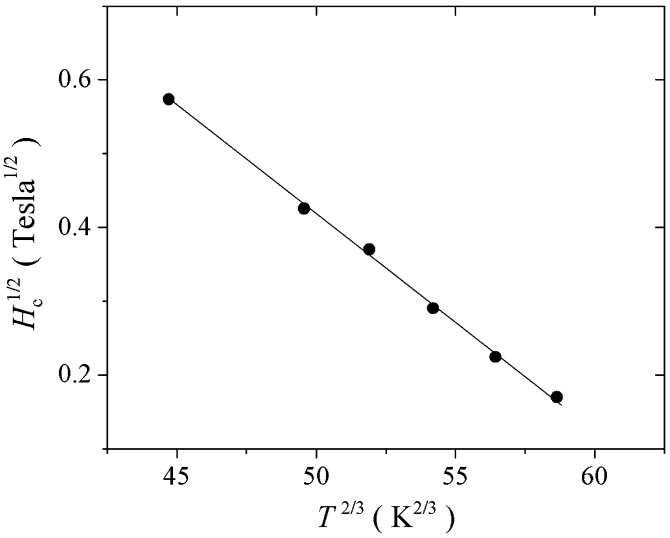

Fig. 8. Fitting of $H_c(T)$ data to Eq. (9) within the range 300–463 K. The line was fitted as: $H_c^{1/2} = 1.8656$ [T$^{1/2}$]–0.0289$T^{2/3}$ [T$^{1/2}$ K$^{-2/3}$].

[21]). In addition, the domain wall width $\delta_w = 4b$ can also be determined from the slope of the fitted $H_c(T)$ equation as follows:

$$\delta_w = \frac{75 k_B H_0^{3/4}}{f(0.0289)^{3/2}} \tag{11}$$

The restoring force term f is proportional to the interaction energy E_m between the domain wall of a single defect, and inversely proportional to the domain wall width δ_w [26], i.e. $f = E_m/\delta_w$. For a spherical defect of radius r fully immersed within a domain region, E_m is of magnetostatic character, and therefore: $E_m = N_d \times M_s^2/2$, where N_d corresponds to the demagnetising factor of a sphere ($N_d = 1/3$, SI). Then, the total energy can be written as $E_m = (1/3)(M_s^2/\mu_0)(4\pi r^3/3) = 2\pi M_s^2 r^3/9\mu_0$. When the domain wall bisects the spherical defect, E_m becomes half partitioned, so that $E_{m,2} = \pi M_s^2 r^3/9\mu_0$. From the strong pinning criterion of the Gaunt model, it is necessary to have $2r > \delta_w$. Assuming $\delta_w = r$ as the maximum δ_w length, we have for the maximum restoring force $f = \pi M_s^2 r^3/9\mu_0 r = \pi M_s^2 r^2/9\mu_0$. For this expression with $\mu_0 M_s = 0.77$ T and $r = 20 \times 10^{-9}$ m, we have $f = 6.59 \times 10^{-11}$ N, and thus from Eq. (11) a DW width value of $\delta_w = 8.14$ nm. This δ_w is in good agreement with the estimated value by MFM analysis (Fig. 7).

According to Eq. (10), the DW surface energy γ can have a maximum value of

$$\gamma < \frac{3f}{2\pi\delta_w} = 3.86x10^{-3}\left[\frac{J}{m^2}\right] \tag{12}$$

And thus, an estimation of the alloy's exchange constant A and the anisotropy constant K, are feasible by considering the relationship between δ_w, γ, A and K for a 180° DW [17]

$$\delta_w = \pi\sqrt{\frac{A}{K}} \tag{13}$$

$$\gamma = 4\sqrt{AK} \tag{14}$$

which leads to the maximum values $A = 2.50 \times 10^{-12}$ J/m and $K = 3.72 \times 10^5$ J/m^3. This anisotropy constant is typical of a hard phase, since it is comparable with, for instance, the K of hexaferrites like $BaFe_{12}O_{19}$ ($K = 3.2 \times 10^5$ J/m^3) [27]. These results are also in excellent agreement with the A, K values (2.0×10^{-12} J/m and 3.3×10^5 J/m^3, respectively) determined for the related as-cast/annealed $Nd_{60}Fe_{20}Co_{10}Al_{10}$ bulk alloys [20].

5. Conclusion

Pinning of domain walls was consistent with the temperature variation of coercivity in composite $Nd_{60}Fe_{30}Al_{10}$ bulk alloys, from which the estimation of the anisotropy constant resulted in the order of 10^5 J/m^3, typical of a hard magnetic phase. The magnetic domains formation were ascribed to the exchange coupling between ferromagnetic clusters, homogeneously distributed within the amorphous phase, which in turn, presents a ferromagnetic–superferromagnetic, superferromagnetic–paramagnetic transitions at $T_1 = 473$ K and $T_2 = 553$ K, respectively.

Acknowledgments

The authors are grateful to Gabriel Lara, Omar Novelo and Carlos Flores for their valuable technical assistance during the alloys preparation and characterisation.

References

[1] H. Chiriac, N. Lupu, in: Y. Liu, D.J. Sellmyer, D. Shindo (Eds.), Handbook of Advanced Magnetic Materials, vol. 3, Springer-Tsinghua University Press, New York, 2006, p. 303.
[2] S. Ram, Curr. Sci. 86 (2004) 832.
[3] H. Chiriac, N. Lupu, Phys. B 299 (2001) 293.
[4] A. Inoue, A. Takeuchi, T. Zhang, Metall. Mater. Trans. A 29A (1998) 1779.
[5] A. Inoue, Bulk Amorphous Alloys. Practical Characteristics and Applications, Trans Tech Publications LTD., Switzerland, 1999, p. 64.
[6] Y. Li, J. Ding, S.C. Ng, X.Z. Wang, J. Magn. Magn. Mater. 187 (1998) L273.
[7] X.Z. Wang, Y. Li, J. Ding, L. Si, H.Z. Kong, J. Alloys Compd. 290 (1999) 209.
[8] L. Wang, J. Ding, Y. Li, Y.P. Feng, X.Z. Wang, N.X. Phuc, N.H. Dan, J. Magn. Magn. Mater. 224 (2001) 143.
[9] G. Ausanio, H. Chiriac, U. Iannotti, C. Hison, L. Lanotte, N. Lupu, J. Magn. Magn. Mater. 265 (2003) 138.
[10] C.E. Rodriguez Torres, A.F. Cabrera, F.H. Sanchez, O.V. Billoni, S.E. Urreta, L.M. Fabietti, J. Magn. Magn. Mater. 267 (2003) 92.
[11] L. Wang, J. Ding, H.Z. Kong, Y. Li, Y.P. Feng, Phys. Rev. B 64 (2001) 214410.
[12] R.J. Ortega-Hertogs, A. Inoue, K.V. Rao, Scr. Mater. 44 (2001) 13333.
[13] L. Wang, J. Ding, Y. Li, Y.P. Feng, N.X. Phuc, N.H. Dan, J. Appl. Phys. 89 (2001) 8046.
[14] N. Lupu, H. Chiriac, A. Takeuchi, A. Inoue, J. Magn. Magn. Mater. 272–276 (2004) e1137.
[15] Z.G. Sun, W. Löser, J. Eckert, K.-H. Müller, L. Schultz, J. Magn. Magn. Mater. 261 (2003) 122.
[16] G. Kumar, K. Eckert, S. Roth, K.-H. Müller, L. Schultz, J. Alloys Compd. 348 (2003) 309.
[17] S. Chikazumi, Physics of Ferromagnetism, second ed, Clarendon Press, Oxford, 1997, p. 191.
[18] S. Yoshiike, H. Adachi, H. Ichinose, K. Tokumitsu, H. Ino, K. Siratori, Mater. Trans., JIM 39 (1998) 102.
[19] L. Wang, J. Ding, Y. Li, H.Z. Kong, Y.P. Feng, X.Z. Wang, J. Phys.: Condens. Matter 12 (2000) 4253.
[20] L. Wang, J. Ding, Y. Li, Y.P. Feng, N.X. Phuc, N.H. Dan, J. Appl. Phys. 89 (2001) 8046.
[21] R. Sato Turtelli, D. Triyono, R. Grossinger, H. Michor, J.H. Espina, J.P. Sinnecker, H. Sassik, J. Eckert, G. Kumar, Z.G. Sun, G.J. Fan, Phys. Rev. B 66 (2002) 054441.
[22] P. Min Xiang, W. Bing Chen, X. Lei, W. Weihua, Z. Dequian, Z. Zhi, H. Bao Shan, Intermetallics 10 (2002) 1215.
[23] M.J. Kramer, A.S. O'Connor, K.W. Dennis, R.W. McCallum, L.H. Lewis, L.D. Tung, N.P. Duong, IEEE Trans. Magn. 37 (2001) 2497.
[24] B.C. Wei, W.H. Wang, M.X. Pan, B.S. Han, Z.R. Zhang, W.R. Hu, Phys. Rev. B 64 (2001) 012406.
[25] P. Gaunt, Philos. Mag. B 48 (1983) 261.
[26] G. Berttoti, Hysteresis in Magnetism, Academic Press, San Diego, 1998, p.361.
[27] H. Kronmuller, M. Fahnle, Micromagnetism and the Microstructure of Ferromagnetic Solids, Cambridge University Press, UK, 2003, p.22.